IEEE Access
Multidisciplinary | Rapid Review | Open Access Journal

Received 26 December 2021, accepted 17 January 2022, date of publication 26 January 2022, date of current version 28 February 2023.

Digital Object Identifier 10.1109/ACCESS.2022.3146713

REGULAR

Intelligent Prediction Method for Heat Dissipation State of Converter Heatsink

HAO JIA[1], JIE CHEN[1], (Member, IEEE), HEPING FU[1], (Student Member, IEEE), RUICHANG QIU[1], AND ZHIGANG LIU[2]

[1]School of Electrical Engineering, Beijing Jiaotong University, Beijing 100044, China
[2]Beijing Rail Transit Electrical Engineering Technology Research Center, Beijing 100044, China

Corresponding author: Jie Chen (jiechen@bjtu.edu.cn)

This work was supported by the Fundamental Research Funds for the Central Universities under Grant 2020JBM063.

ABSTRACT Currently, the offline manual periodic detection method is a well-established practice in detecting the thermal state of the converter heatsink. This method, however, is huge in maintenance costs. To lower maintenance costs and improve maintenance efficiency in detecting the thermal dissipation state, this paper proposes an intelligent online prediction scheme based on Gauss-Newton iteration method. Firstly, the power loss model of the power module is established according to the characteristics of IGBT and FWD. The power loss of the power device is then calculated in real time with the voltage and current parameters of the converter. Next, the transient thermal model of the heatsink is established based on thermodynamics theory. And the calculation method of steady thermal resistance of heatsink based on Gauss-Newton iteration method is proposed according to the model. The transient thermal impedance data allow for timely prediction of thermal resistance of the heatsink and characterize the thermal state of the heatsink. Finally, with the help of DSP28377D, an experimental platform is built to verify the scheme. Results show that this method can realize intelligent prediction of thermal state online.

INDEX TERMS Power electronic converters heatsink intelligent prediction Gauss-Newton iteration method.

I. INTRODUCTION

The trend of increasing power densities of modern-day power converters is pushing power devices to their thermal limits [1]. Failures of power devices are mostly caused by thermal stress [2]. Therefore, the thermal dissipation potential of the heatsink is critical to ensuring the long-term stable operation of power devices [3]. Currently, the forced air-cooled system takes a dominant position in the thermal management of power devices, thanks to its low cost, good heat dissipation, high reliability, and ease of implementation [4]. However, in practical application, forced air cooling heatsink will inevitably be blocked by some dust and debris, reducing the heat dissipation efficiency [5]. The blocked air outlets of the heatsink are mainly maintained as planned, which is ''blind'' and generates considerable maintenance costs. To reduce maintenance costs and improve maintenance efficiency, it is urgent to study repair according to the condition of the heatsink.

The associate editor coordinating the review of this manuscript and approving it for publication was Gab-Su Seo.

To date, the prediction method about the heat dissipation state of the heatsink is rarely researched. Most researchers direct their attention to heatsinks analysis and design. [6] designed an algorithm for calculating switching loss and junction temperature of switching elements in PSIM, to judge whether the heatsink meets the heat dissipation requirements. It provided an idea of calculating power loss when it is impossible to measure the voltage drop on switching elements. [7] built the RC parameter model of IGBT and heatsink by analyzing the thermal network, to obtain the temperature of the IGBT module, which provided a reference for thermal analysis about the cooling system. [8] proposed a thermal coupling resistances network model, established the relationships between the case-to-ambient thermal resistance of individual power devices and their thermal coupling resistance to the adjacent device. It provides a better understanding of the thermal behavior of power devices.

To analyze the heat dissipation potential of a heatsink, [9] and [10] studied the thermal transmission of the heatsink and described the relationship between the performance of forced air-cooled heatsink and airflow rate and heat transfer

surface area. [11] established a thermal model of air cooling fin heatsink based on finite difference method, and realized the estimation of fin temperature with given heatsink parameters. The above literature has studied the thermal dissipation potential of a heatsink, which provides an insight into the analysis of analyzing heat dissipation potential in normal operation. But there is a lack of research on the heat dissipation potential of the heatsink after failures.

In terms of heatsink degradation, [12] found that a critical reason for the deterioration of the heatsink is that when heatsink was exposed to the external environment, some dust and dirt adhere to the fin of the heatsink and form an insulation layer and affecting heat dissipation. [13] found that the main reason for heatsink performance degradation was the accumulation of dust in the air inlet, which reduced the airflow in the air flue and reduced the heat dissipation effect. [14] studied the influence of dirt on the heatsink and established the relationship between heat resistance and blocking degree of the heatsink. But the accuracy needed to be improved, and the intelligent prediction of the heatsink state is not yet achieved. [15] proposed a strategy to evaluate the effectiveness of a test procedure for checking the correct assembling and behavior of heatsinks for power devices is proposed. However, it only takes the specified thermal resistance change as the fault to obtain the junction temperature curve to judge the status of power devices. It does not consider how to get the thermal resistance. So how to apply it to practical engineering remains to be studied. [16] studied the operation state prediction of the forced air cooling system, but the scheme is an offline monitoring scheme, workable only during the downtime of equipment.

To solve the problems such as low accuracy and offline detection in predicting the thermal dissipation state of the heatsink, this paper proposes a real-time heatsink state prediction scheme based on thermal resistance. First, based on the thermal model of the heatsink, the steady temperature of the heatsink is predicted by Gauss-Newton iteration scheme with heatsink temperature and ambient temperature. Then the thermal resistance of the heatsink is calculated with the temperature on steady-state and power loss. Finally, the blocking degree is predicted. And this scheme involves no sensor.

II. SOLUTION FOR PREDICTING HEAT DISSIPATION STATE ONLINE

To avoid the failure of power devices caused by thermal stress and lower maintenance costs, this paper proposes an intelligent online prediction scheme that can support repair according to condition. This paper first analyzes the parameters which can reflect the condition of the heatsink and select thermal resistance as a key parameter. Then according to the definition of thermal resistance, this paper solves all the required variables to calculate thermal resistance. In this process, an algorithm to calculate steady-state temperature is proposed based on Gauss-Newton iteration method. Finally, this paper establishes the relation between thermal resistance and blocking degree.

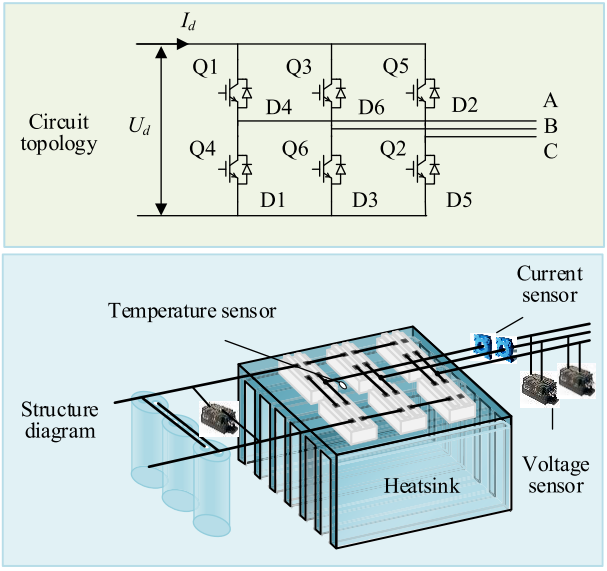

FIGURE 1. Inverter topological diagram.

Fig. 1 shows our research object, a three-phase inverter that relies on a forced air-cooled system for thermal dissipation. The heat source serves as the only IGBT module.

Thermal resistance, as a physical quantity about heat transfer capacity, can characterize the ability of heating power to cause temperature changes [17]. The thermal resistance of the heatsink includes base plate thermal resistance, thermal conduction resistance of fins, and thermal convection resistance of fins. The thermal resistance of the base plate and thermal conduction resistance of fins mainly depends on the material and size of the heatsink. The thermal convection resistance of fins is affected by air velocity and convective heat transfer area [18]. When the heatsink is blocked, the airflow through the heatsink and the convective heat transfer area decreases, so that the heat transfer efficiency of heatsink fins decreases, and the thermal resistance becomes larger [19]. It shows that thermal resistance can effectively characterize the working conditions of the heatsink. Therefore, this article uses thermal resistance to infer the heat dissipation state of the heatsink.

The calculation formula of thermal resistance is as follows.

$$Z_{\mathrm{hs}}(t) = \frac{\Delta T_{\mathrm{hs}}(t)}{P(t)} \tag{1}$$

where P(t) is the power loss of the power device, Z_{hs}(t) is the thermal resistance of the heatsink, and ΔT_{hs}(t) is the temperature rise of the heatsink relative to ambient temperature.

As the blocking degree of the heatsink increases, the thermal resistance grows stronger, causing the heatsink to vary in temperature. The heatsink temperature needs time to stabilize. We cannot directly solve actual thermal resistance with transient temperature [20]–[22]. In addition, due to the large heat capacity of the heatsink, it takes a long time for heatsink temperature to stabilize. Therefore, it is difficult to judge the sudden blockage (such as the blockage caused by plastic bags on high-speed rail) if we wait until the heatsink temperature is steady.

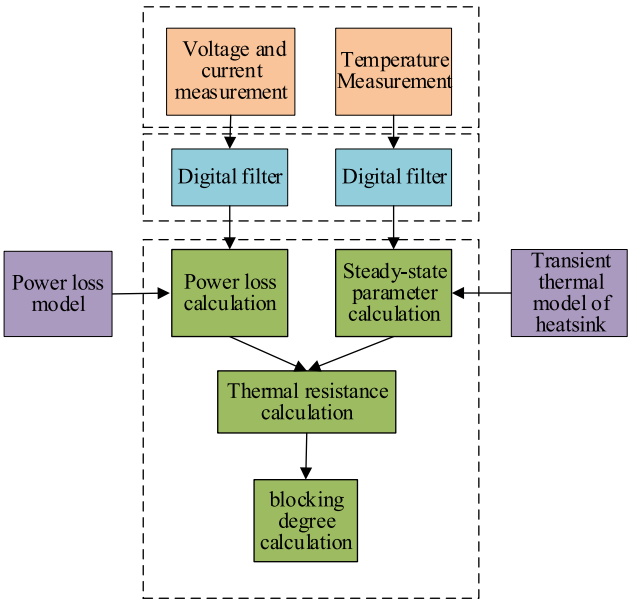

FIGURE 2. Radiator condition monitoring flow chart.

To this end, this paper establishes a heatsink thermal resistance model including the power loss model of the power device and transient heat model of the heatsink. Then it uses short-term data on transient-state to solve heatsink thermal resistance based on Gauss-Newton iteration method, thereby inferring the blocking degree of the heatsink.

Fig. 2 shows the flow chart of the online prediction scheme for the heat dissipation state of the heatsink proposed in this paper. Firstly, the power loss model and the transient heat model are derived. Critical data is then obtained through the existing sensor and filtered by a digital filter. After that, the parameters on steady state are solved based on Gauss-Newton iteration method, then the actual thermal resistance is calculated, and the blocking degree of the heatsink is finally obtained. This scheme allows us to calculate the blockage degree without adding any new sensors.

III. THERMAL IMPEDANCE MODEL OF HEATSINK

According to (1), we need power loss and temperature rise to solve thermal resistance. To achieve this end, we establish the power loss model and the transient thermal model in this section.

A. POWER LOSS CALCULATION MODEL

The inverter adopts SVPWM modulation. Considering the symmetry of the circuit, the power loss of each IGBT and its FWD are the same. Therefore, the power loss is solved only for IGBT Q1 and FWD D4, which are on the upper half-bridge arm of phase A.

Q1 and D4 have different conduction times in sectors of SVPWM. And the sectors, which the SVPWM reference voltage passes through, are affected by power factor angle. In SVPWM modulation, IGBT only circulates

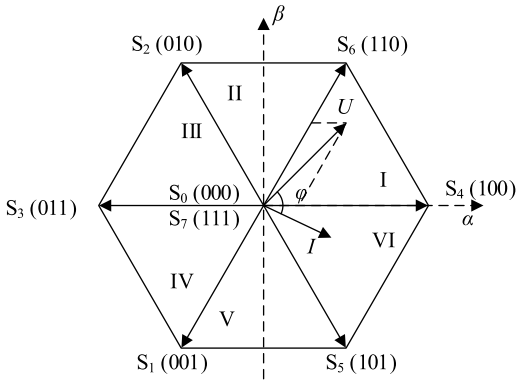

FIGURE 3. Voltage vector diagram of SVPWM.

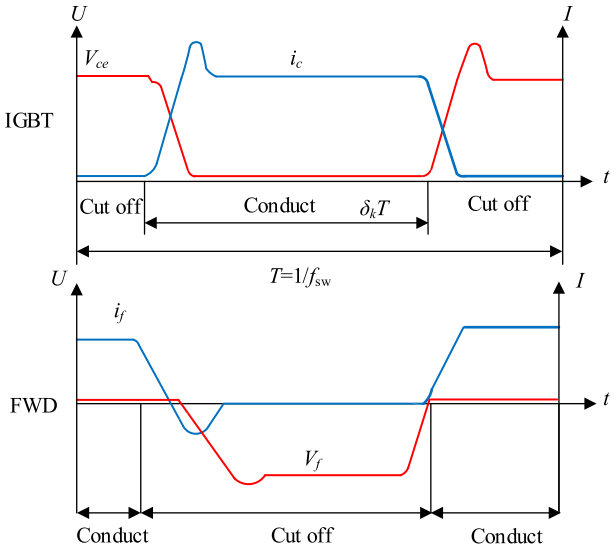

FIGURE 4. IGBT and diode voltage and current schematic diagram.

forward current. According to the voltage vector diagram of SVPWM (Fig. 3), the phase angle of forward current covers $[-\pi/2,\pi/2]$. When the power factor Angle φ is at $[0,\pi/6]$, the reference voltage passes through four sectors: I, II, V, and VI. When the power factor Angle φ is at $[\pi/6,\pi/2]$, the reference voltage passes through other four sectors: I, II, III, and VI.

Assuming that the ac power factor Angle φ is at $[0,\pi/6]$, and the reference voltage of SVPWM passes through four sectors: I, II, V, and VI. FIG. 4 shows the voltage and current waveform of IGBT and FWD within one switching cycle. A switching period includes the time of conduction, cut-off, and switch state. The conduction loss of IGBT and FWD cannot be ignored for the drop in conduction voltage. The cut-off loss, however, can be ignored since the offset current of IGBT and FWD in the cut-off state is very small. Switching loss occurs in the switch state since the voltage and current cannot switch to zero instantly.

The power loss of IGBT includes conduction loss $P_{\text{cond\_Q1}}$ and switching loss $P_{\text{sw\_Q1}}$ [23]. Their calculation is

shown in (2) and (3).

$$\begin{aligned} P_{\text{cond\_Q1}} = & \frac{1}{2\pi}\int_0^{\frac{\pi}{3}} v_{\text{ce}}(t)\cdot i_{\text{c}}(t)\cdot\delta_1 d\omega t \\ & + \frac{1}{2\pi}\int_{\frac{\pi}{3}}^{\frac{\pi}{2}+\varphi} v_{\text{ce}}(t)\cdot i_{\text{c}}(t)\cdot\delta_2 d\omega t \\ & + \frac{1}{2\pi}\int_{-\frac{\pi}{2}+\varphi}^{-\frac{\pi}{3}} v_{\text{ce}}(t)\cdot i_{\text{c}}(t)\cdot\delta_5 d\omega t \\ & + \frac{1}{2\pi}\int_{-\frac{\pi}{3}}^{0} v_{\text{ce}}(t)\cdot i_{\text{c}}(t)\cdot\delta_6 d\omega t \end{aligned} \tag{2}$$

$$P_{\text{sw\_Q1}} = f_{\text{sw}}\cdot\frac{1}{\pi}\cdot\left(E_{\text{on}}(i_c)+E_{\text{off}}(i_c)\right) \tag{3}$$

The power loss of FWD is also composed of conduction loss $P_{\text{cond\_D4}}$ and switching loss $P_{\text{sw\_D4}}$ [24]. The calculation is shown in (4) and (5).

$$\begin{aligned} P_{\text{cond\_D4}} = & \frac{1}{2\pi}\int_0^{\frac{\pi}{3}} v_{\text{f}}(t)\cdot i_{\text{f}}(t)\cdot(1-\delta_1) d\omega t \\ & + \frac{1}{2\pi}\int_{\frac{\pi}{3}}^{\frac{\pi}{2}+\varphi} v_{\text{f}}(t)\cdot i_{\text{f}}(t)\cdot(1-\delta_2) d\omega t \\ & + \frac{1}{2\pi}\int_{-\frac{\pi}{2}+\varphi}^{-\frac{\pi}{3}} v_{\text{f}}(t)\cdot i_{\text{f}}(t)\cdot(1-\delta_5) d\omega t \\ & + \frac{1}{2\pi}\int_{-\frac{\pi}{3}}^{0} v_{\text{f}}(t)\cdot i_{\text{f}}(t)\cdot(1-\delta_6) d\omega t \end{aligned} \tag{4}$$

$$P_{\text{sw\_D4}} = f_{\text{sw}}\cdot\frac{1}{\pi}\cdot E_{\text{rr}}(i_{\text{f}}) \tag{5}$$

where ω is the angular frequency of reference voltage, i_{c} is the current flowing through IGBT, i_{f} is the current flowing through FWD; V_{ce} is the voltage drop between the collector and emitter of IGBT, V_{f} is the voltage drop of FWD; f_{sw} is the switching frequency of IGBT, and δ is the duty cycle; i_{c} and i_{f} can be obtained by using the current sensor to measure the ac current of the inverter; V_{ce} and V_{f} can be calculated with the help of the UI characteristic curve; E_{on} refers to turn-on loss of IGBT, E_{off} refers to turn-off loss of IGBT, and E_{rr} refers to turn-off loss of FWD.

According to (2) - (5), the duty cycle of IGBT and FWD is needed to solve power loss. Take reference voltage in the first sector as an example, the duty cycle δ_1 of Q1 is calculated as below.

According to the voltage vector diagram in the first sector, the acting time of the primary and secondary vectors can be calculated through vector decomposition.

$$T_4 = \text{m}\cdot\sin(\frac{\pi}{3}-\theta)\cdot T_s \tag{6}$$

$$T_6 = \text{m}\cdot\sin(\theta)\cdot T_s \tag{7}$$

Combined with the on-off state of IGBT in each vector, the duty cycle of Q1 can be calculated.

$$\delta_1 = \left(T_4+T_6+\frac{1-T_4-T_6}{2}\right)/T_s = \frac{1}{2}\left(1+\text{m}\cos\left(\theta-\frac{\pi}{6}\right)\right) \tag{8}$$

TABLE 1. Duty cycle of Q1 and D4.

Sector	Duty cycle of Q1	Duty cycle of D4
I	(1+mcos(θ-π/6))/2	(1-mcos(θ-π/6))/2
II	(1+$\sqrt{3}$ mcosθ)/2	(1-$\sqrt{3}$ mcosθ)/2
III	(1+mcos(θ+π/6))/2	(1-mcos(θ-π/6))/2
IV	(1+mcos(θ-π/6))/2	(1-mcos(θ+π/6))/2
V	(1+$\sqrt{3}$ mcosθ)/2	(1-$\sqrt{3}$ mcosθ)/2
VI	(1+mcos(θ+π/6))/2	(1-mcos(θ+π/6))/2

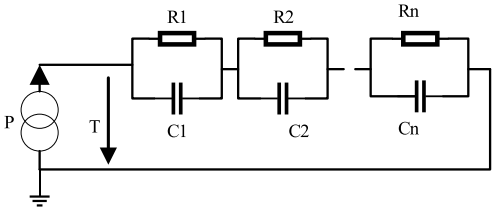

FIGURE 5. Foster model diagram.

Similarly, the duty cycle of Q1 in other sectors can be calculated. The duty cycle of Q1 and D4 are complementary. The duty cycle of Q1 and D4 in all sectors is shown in Table 1.

After calculating the duty cycle, we can solve $P_{\text{cond\_Q1}}$, $P_{\text{sw\_Q1}}$, $P_{\text{cond\_D4}}$, and $P_{\text{sw\_D4}}$ with (2) to (5). The total power loss of the inverter is six times the loss of Q1 and D4.

$$P_0 = 6\cdot\left(P_{\text{cond\_Q1}}+P_{\text{cond\_D4}}+P_{\text{sw\_Q1}}+P_{\text{sw\_D4}}\right) \tag{9}$$

B. THERMAL TRANSIENT MODEL OF HEATSINK

This paper adopted the Foster model for the cooling system modeling. In this model, the change of the reference point will not affect the thermal resistance and heat capacity before the reference point. We only need to cascade the thermal network after the reference point. This model simplifies the thermal network. It is more accurate and more popular with researchers [25].

The power loss generated by the inverter is converted to heat. Part of the heat is dissipated to the ambiance by the heatsink, and the rest increases heatsink temperature.

Note that P_0 is the power loss that is converted to heat, and ϕ is the instantaneous heat flow rate of the heatsink. According to the conservation law of energy:

$$P_0 = h_{\text{fin}}\cdot A\cdot\Delta T_{\text{hs}}(t)+\phi\cdot V \tag{10}$$

where V is the volume of the heatsink, in m^3; A is the convective heat transfer surface area of the heatsink, in m^2; h_{fin} is the convective heat transfer coefficient, in W/($\text{m}^2\cdot$°C).

The transient heat equation about internal heat source is:

$$\frac{d(\Delta T_{\text{hs}}(t))}{dt} = \frac{\phi}{\rho c} \tag{11}$$

where c is the heat capacity, in J/ (kg·°C); ρ is the density of heatsink, in kg/m^3; t is time, in s.

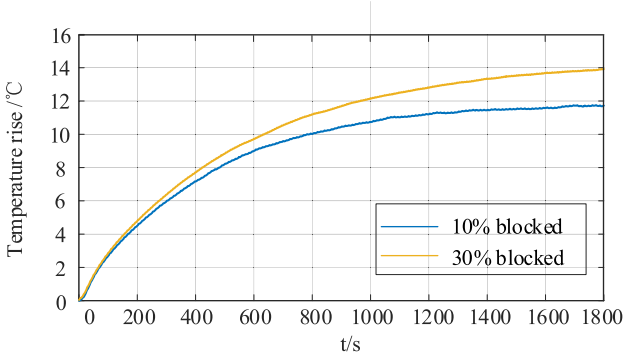

FIGURE 6. A heatsink real-time temperature rise relative to ambient temperature under different blockage conditions.

Combined with (10) and (11), the differential equation about heatsink temperature can be obtained:

$$\rho cV\frac{d\left(\Delta T_{\mathrm{hs}}\left(t\right)\right)}{dt}=-h_{\mathrm{fin}}\cdot A\cdot\Delta T_{\mathrm{hs}}\left(t\right)-T_{\mathrm{a}}\left(t\right)+P_0 \quad (12)$$

By solving (12), the expression of heatsink temperature can be calculated. Assuming that the initial conditions of the differential equation are $t = t_0$, $\Delta T_{\mathrm{hs}} = \Delta T_{\mathrm{hs}}(t_0)$. The solution of this equation is given in equation (13).

$$\Delta T_{\mathrm{hs}}(t) = \Delta T_{\mathrm{hs}}\left(t_0\right) + \left(\Delta T_{\mathrm{hs}}\left(\infty\right) - \Delta T_{\mathrm{hs}}\left(t_0\right)\right)\left(1-e^{-\frac{t-t_0}{\tau_{\mathrm{hs}}}}\right) \quad (13)$$

where $\tau_{\mathrm{hs}} = 1/R_{\mathrm{hs}}C_{\mathrm{hs}}$, is time constant; $R_{\mathrm{hs}} = 1/Ah_{\mathrm{fin}}$, is the actual thermal resistance of the heatsink; $C_{\mathrm{hs}} = \rho cV$, is heat capacity of the heatsink; $\Delta T_{\mathrm{hs}}(\infty) = P_0R_{\mathrm{hs}}$, is the temperature rise on steady state, which is the temperature rise at $t = \infty$.

(14) is the expression of thermal resistance calculated with (13) and (1).

$$Z_{\mathrm{hs}}(t) = Z_{\mathrm{hs}}\left(t_0\right) + \left(R_{\mathrm{hs}} - Z_{\mathrm{hs}}\left(t_0\right)\right)\left(1-e^{-\frac{t-t_0}{\tau_{\mathrm{hs}}}}\right) \quad (14)$$

Blocking degree changes of heatsink will lead to changes about thermal resistance, which is reflected as changes about R_{hs} and τ_{hs} in (13). Fig. 6 is the schematic drawing of heatsink temperature at different blocking degrees.

According to (13) and (14), the transient heatsink temperature and the thermal resistance calculated with equation (1) change slowly to steady state in exponential form, where the constant term is steady-state temperature and actual thermal resistance. The time constant is composed of thermal resistance and heat capacity. In practice, it takes a long time for the temperature to stabilize. So the actual thermal resistance cannot be directly calculated with transient temperature, so a method to predict the steady-state temperature and the actual thermal resistance is needed.

IV. STEADY-STATE PARAMETER SOLUTION BASED ON GAUSS-NEWTON ITERATION METHOD

To calculate the actual thermal resistance with transient temperature, an algorithm based on Gauss-Newton iteration method is proposed.

Gauss-Newton iteration method is mainly used to calculate parameters in nonlinear regression model [26]. It obtains an approximate linear model using Taylor expansion. The deviation between the theoretical value and the actual value is used to correct the parameter's value. Gauss-Newton iteration method includes initial value selection, Jacobian matrix solution, parameter correction, and accuracy test [27].

We can obtain a new expression by sorting out (13):

$$y = f(t) = \Delta T_{\mathrm{hs}}\left(\infty\right) + \left(\Delta T_{\mathrm{hs}}\left(t_0\right) - \Delta T_{\mathrm{hs}}\left(\infty\right)\right)e^{-\frac{t}{\tau_{\mathrm{hs}}}} \quad (15)$$

The parameters to be calculated are temperature rise on steady state $\Delta T_{\mathrm{hs}}(\infty)$, the initial temperature rise $\Delta T_{\mathrm{hs}}(t_0)$, and time constant τ_{hs}. Note the above parameters a_0, a_1, a_2 in order. Their initial values are $a^{(0)} = (a_0^{(0)}, a_1^{(0)}, a_2^{(0)})^{\mathrm{T}}$. The initial values are set empirically and affect the convergence of iteration.

Taylor expansion is performed on (15) at $a^{(0)}$, where the second and higher-order terms are omitted to obtain an approximate linear expression:

$$f\left(t_i, a\right) \approx f\left(t_i, a^{(0)}\right) + \sum_{k=0}^{2}\left[\frac{\partial f\left(t_i, a\right)}{\partial a_k}\right]_{a=a^{(0)}}\left(a_k - a_k^{(0)}\right) + \varepsilon_i \quad (16)$$

Partial derivatives of the parameters are:

$$\frac{\partial f}{\partial a_1} = 1 - e^{-\frac{t}{\tau_{\mathrm{hs}}}} \quad (17)$$

$$\frac{\partial f}{\partial a_2} = -e^{-\frac{t}{\tau_{\mathrm{hs}}}} \quad (18)$$

$$\frac{\partial f}{\partial a_3} = \frac{(a_0 - a_1)}{\tau_{\mathrm{hs}}}e^{-\frac{t}{\tau_{\mathrm{hs}}}} \quad (19)$$

Set

$$\Delta y_i^{(0)} = y_i - f\left(t_i, a^{(0)}\right) \quad (20)$$

$$\Delta a_k^{(0)} = a_k - a_k^{(0)} \quad (21)$$

$$J_{ik}^{(0)} = \sum_{k=0}^{2}\left[\frac{\partial f\left(t_i, a\right)}{\partial a_k}\right]_{a=a^{(0)}} \quad (22)$$

(16) can be simplified as:

$$\Delta y_i^{(0)} = J_{ik}^{(0)}\Delta a_k^{(0)} + \varepsilon_i \quad (23)$$

The matrix form of (23) is (24), where $\mathbf{J}^{(0)}$ is the Jacobian matrix:

$$\Delta \mathbf{Y}^{(0)} = \mathbf{J}^{(0)}\Delta \mathbf{A}^{(0)} + \mathbf{E} \quad (24)$$

Corrected parameter values are calculated with the Jacobian matrix by the least square method:

$$\Delta \mathbf{A}^{(0)} = \left(\mathbf{J}^{(0)^{\mathrm{T}}}\mathbf{J}^{(0)}\right)^{-1}\mathbf{J}^{(0)^{\mathrm{T}}}\Delta \mathbf{Y}^{(0)} \quad (25)$$

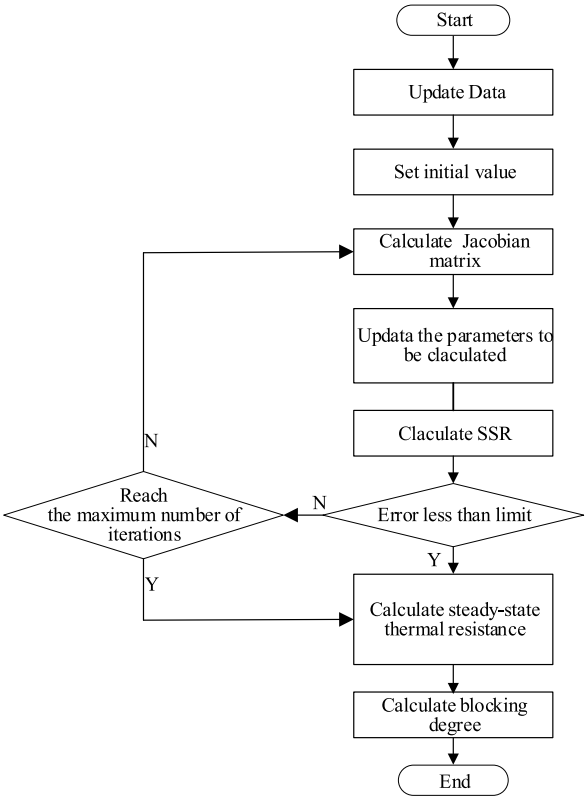

FIGURE 7. Flow chart of prediction algorithm.

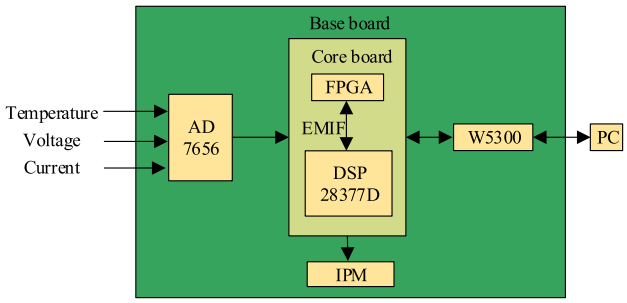

FIGURE 8. Architecture block diagram of the experimental platform.

TABLE 2. Parameters of experimental platform.

Name	Parameter	Name	Parameter
Dc rated voltage/V	400	Power factor	0.9
Dc rated current/A	20	AD sampling frequency/Hz	5000
Dc rated power/W	8000	Heatsink type	Steel aluminum fin radiator
Modulation	SVPWM	Heatsink size L*W*H/cm	30*19*9
Switching frequency /Hz	5000	Fan type	MGA8024UB-O25
Modulation ratio	0.8	Number of fans	2

Whether the results meet the requirements is judged with the sum of squares of residuals. If it is within the error limit, the iteration will cease. The formula for calculating the sum of squares of residuals is as follows:

$$SSR = \sum_{i=0}^{n} \left[y_i - f\left(t_i, a^{(i)}\right) \right]^2 \tag{26}$$

In addition, the maximum number of iterations is set. If the sum of squares of residuals still fails to meet the requirements after too many iterations, the iteration can still be stopped to prevent iteration stuck.

The algorithm flow chart is shown in Fig. 7.

With the help of this algorithm, the steady temperature can be calculated with transient temperature, and the actual thermal resistance can be calculated by combining the power loss obtained before, and the blocking degree can be obtained.

This method is featured by simple implementation, high calculation accuracy, fast calculation speed, and no additional sensors. It can ensure good prediction accuracy and good real-time performance.

V. VERIFICATION

A. EXPERIMENT PLATFORM INFORMATION

In this paper, an experimental platform is built based on DSP28377D. The framework of the experimental platform is shown in Fig. 8, and the parameters are shown in Table 2. The IPM adopts SVPWM modulation, and the load is a resistive load in star connection. We use voltage and current sensors to measure the ac line voltage, ac line current, use PT1000 to obtain the heatsink temperature and ambient temperature, and use W5300 to transmit AD sampling data and results to PC.

B. PREDICTION RESULTS

First, power loss is calculated with measured voltage and current. Next, according to the real-time temperature measured, the steady temperature is solved based on Gauss-Newton iteration method. Then the thermal resistance was calculated with temperature on steady state, ambient temperature, and power loss. Finally, the blocking degree is obtained with the relationship between thermal resistance and blocking degree. The iterative array stores 1800 temperature data in the last 180 seconds at 0.1-second intervals. The steady temperature and thermal resistance are calculated with the data periodically, and the predicted value of blocking degree is calculated periodically.

Experiments are carried out on the experiment platform at the interval of 10% blockage degree, and experiments cover the conditions of 0-100% blockage degree. Table 4 is the thermal resistance calculated with heatsink temperature and ambient temperature and power loss under different blocking degrees.

Fig. 9 shows the relationship between blocking degree and thermal resistance. As shown in Fig. 9, as the blockage increases, the thermal resistance increases. Because the

TABLE 3. Thermal resistance under different blockage conditions.

Blocking degree	Thermal resistance/°C/W	Blocking degree	Thermal resistance/°C/W
0%	0.0458	60%	0.0683
10%	0.0489	70%	0.0802
20%	0.0525	80%	0.0898
30%	0.0572	90%	0.1080
40%	0.0597	100%	0.1451
50%	0.0653		

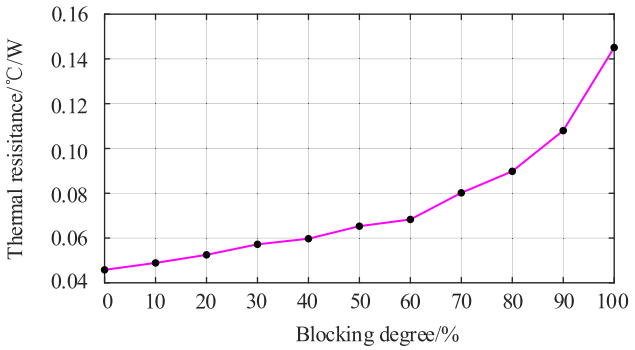

FIGURE 9. Diagram of blocking degree and thermal resistance.

TABLE 4. Prediction results of blocking degree.

Actual blocking degree	Calculated blocking degree	Actual blocking degree	Calculated blocking degree
0%	3%	60%	54%
10%	16%	70%	67%
20%	22%	80%	78%
30%	33%	90%	83%
40%	39%	100%	97%
50%	54%		

blockage deepens, the pressure drop of the heatsink air channel increases. The fans need to provide more pressure to overcome the pressure drop of the air channel, reducing the flow into the radiator and increasing the thermal resistance. In addition, the higher the blockage degree is, the faster the thermal resistance changes. Because the higher the blockage degree is, the faster the pressure drop caused by a blockage in the air channel changes, the faster the airflow changes.

According to the relationship between blocking degree and thermal resistance in Fig. 9, several groups of blocking degree prediction experiments are carried out. Table 5 is the blocking degree prediction results. It shows that the error of this scheme is within 10% blocking degree.

When the blocking degree changes, it takes time for the array to update the data at the new blocking degree, so this scheme needs time to correctly reflect the new blocking degree. At the start of the blocking degree change, the

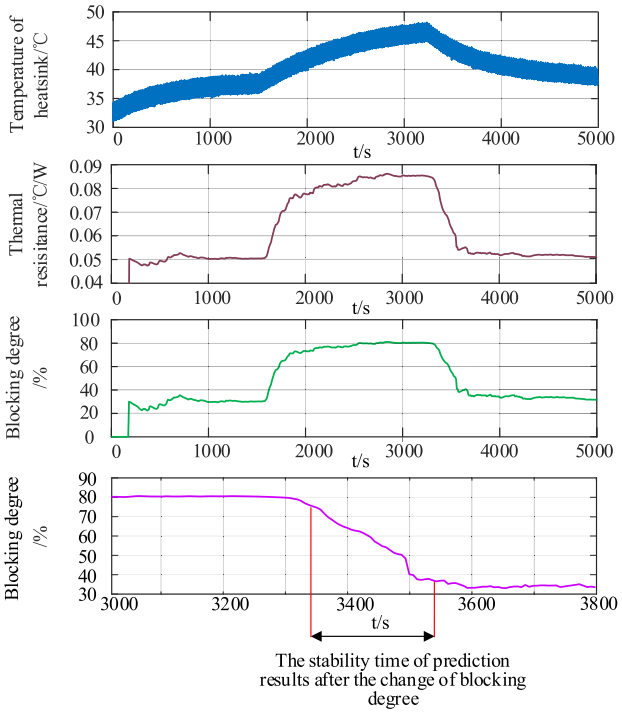

FIGURE 10. Prediction results of blockage condition when blockage changes from 30% to 80% to 30%.

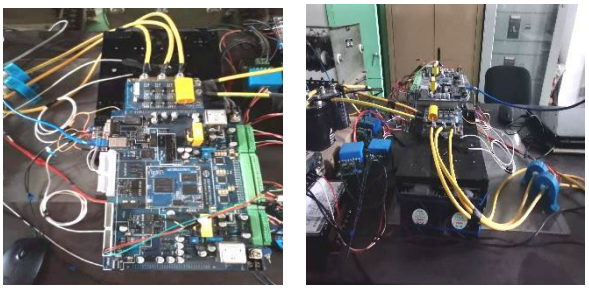

FIGURE 11. Physical drawing of the experimental platform.

blocking degree calculated stays the same because the temperature does not change. As time goes by, when the array contains both data at old blocking degree and data at new blocking degree, the thermal resistance calculated will not be the same as the actual thermal resistance because the parameter to be solved is the thermal resistance of one blocking degree. The thermal resistance calculated will eventually change to the value at new blocking degree as more and more data at new blocking degree are available. During the whole process, the thermal resistance calculated shows a gradual curve. As shown in Fig. 10, the new blocking degree can be predicted in about 3 minutes after blocking degree changes. The waiting time depends on the time contained in the array and the cut-off frequency of the low-pass filter for temperature.

VI. CONCLUSION

This paper proposes a complete method for predicting the blocking degree of heatsink online. In this paper, the power loss of IGBT inverter and the expressions of heatsink

temperature and thermal resistance are obtained by theoretical calculation. Then, based on Gauss-Newton iteration method, the actual thermal resistance is calculated with transient temperature, and the blocking degree is obtained. Finally, DSP28377D is used for data acquisition, transmission, and data process to verify this scheme experimentally. Results show that this scheme can predict the blocking degree of the heatsink with an error of less than 10% within 3 minutes.

REFERENCES

[1] A. Dey, N. Shafiei, R. Khandekhar, W. Eberle, and R. Li, "Lumped parameter thermal network modelling of power transformers," in *Proc. 20th IEEE Intersoc. Conf. Thermal Thermomech. Phenomena Electron. Syst. (iTherm)*, Jun. 2021, pp. 172–178.

[2] Y. Ning, Z. Honggui, and X. Jianxing, "Study on thermal characteristics of power module with double-sided cooling package," *China Light Lighting*, vol. 2, pp. 6–13, Feb. 2021.

[3] L. A. Potapov, A. N. Shkolin, and A. Y. Drakin, "Modeling and control of thermal processes in semiconductor devices," in *Proc. Int. Conf. Ind. Eng., Appl. Manuf. (ICIEAM)*, Mar. 2019, pp. 1–6.

[4] Z. Jian, "Study on heat dissipation structure optimization of power electronic device and equipment," Ph.D. dissertation, Dept. Elect. Eng., HIT Univ., Harbin, China, 2015.

[5] X. Jin, Z. Xinhua, and J. Yanling, "Forced air cooling thermal analysis and optimization," *Power Unit. Chin. J. Electron Devices*, vol. 38, no. 2, pp. 283–286, Apr. 2015.

[6] F. E. Cazakevicius, R. P. Krug, H. H. Figueira, R. C. Beltrame, and H. L. Hey, "Loss and thermal analysis of semiconductor devices applied to an electric circuit simulator," in *Proc. 11th Brazilian Power Electron. Conf.*, Sep. 2011, pp. 1050–1055.

[7] X. Du, T. Li, J. Zhang, H.-M. Tai, P. Sun, and L. Zhou, "Thermal network parameter identification of IGBT module based on the cooling curve of junction temperature," in *Proc. IEEE Appl. Power Electron. Conf. Expo. (APEC)*, Mar. 2016, pp. 2992–2997.

[8] K. Wei, D. D.-C. Lu, C. Zhang, Y. P. Siwakoti, J. L. Soon, and Q. Yao, "Modeling and analysis of thermal resistances and thermal coupling between power devices," *IEEE Trans. Electron Devices*, vol. 66, no. 10, pp. 4302–4308, Oct. 2019.

[9] D. Christen, M. Stojadinovic, and J. Biela, "Energy efficient heat sink design: Natural versus forced convection cooling," *IEEE Trans. Power Electron.*, vol. 32, no. 11, pp. 8693–8704, Nov. 2017.

[10] S. Y. Kim and R. L. Webb, "Analysis of convective thermal resistance in ducted fan-heat sinks," *IEEE Trans. Compon. Packag. Technol.*, vol. 29, no. 3, pp. 439–448, Sep. 2006.

[11] L. Xie, X. Yuan, and W. Wang, "Thermal modeling of fan-cooled plate–fin heatsink considering air temperature rise for virtual prototyping of power electronics," *IEEE Trans. Compon., Packag., Manuf. Technol.*, vol. 10, no. 11, pp. 1829–1839, Nov. 2020.

[12] S. W. Montgomery, "Fouling of high density heat sinks–theoretical origins and numerical analysis," in *Proc. 18th Annu. IEEE Semiconductor Thermal Meas. Manage. Symp.*, Mar. 2002, pp. 132–136.

[13] D. A. Moore, "Characterization of fiber accumulation fouling in fine pitched heat sinks," in *Proc. 25th Annu. IEEE Semiconductor Thermal Meas. Manage. Symp.*, Mar. 2009, pp. 279–284.

[14] A. Nabi, P. Rodgers, and A. Bar-Cohen, "Prediction of thermal performance degradation of air-cooled fine-pitch fin array heat sinks due to fouling," in *Proc. 22nd Annu. IEEE Semiconductor Thermal Meas. Manage. Symp.*, Mar. 2006, pp. 2–9.

[15] D. Piumatti, M. V. Quitadamo, M. S. Reorda, and F. Fiori, "Testing heatsink faults in power transistors by means of thermal model," in *Proc. IEEE Latin-Amer. Test Symp. (LATS)*, Mar. 2020, pp. 1–6.

[16] S. Zheng, X. Du, J. Zhang, and Y. Yu, "Monitoring of the cooling system via thermal parameters," *IEEE Access*, vol. 7, pp. 138110–138121, 2019.

[17] Z. Yanming, Z. Luowei, and L. Hongji, "A numerical algorithm for optimizing dynamic response performance of IGBT heat sinks," *Proc. CSEE*, vol. 36, no. 11, pp. 3017–3026, Mar. 2016.

[18] F. Heping, C. Jie, and J. Hao, "Intelligent detecting method for blockage degree of forced air-cooled heatsinks," *J. Beijing Jiaotong Univ.*, vol. 44, no. 5, pp. 125–132, Oct. 2020.

[19] C. Gammeter, F. Krismer, and J. W. Kolar, "Weight optimization of a cooling system composed of fan and extruded-fin heat sink," *IEEE Trans. Ind. Appl.*, vol. 51, no. 1, pp. 509–520, Feb. 2015.

[20] P. Xiaoyan, "Optimized design of radiator for conberter of EMU," M.S. thesis, Dept. Electron. Eng., Beijing Univ. Civil Eng. s, Beijing, China, 2019.

[21] Q. Dan, "IGBT module radiator design," M.S. thesis, Dept. Electron. Eng., Changsha Univ. Sci. Technol., Changsha, China, 2018.

[22] K. Gorecki and P. Gorecki, "Nonlinear compact thermal model of the IGBT dedicated to SPICE," *IEEE Trans. Power Electron.*, vol. 35, no. 12, pp. 13420–13428, Dec. 2020.

[23] S. Jingwen, "Research on the loss models of high-power photovoltaic inverter," M.S. thesis, Dept. Electron. Eng., Southwest Jiaotong Univ., Chengdu, China, 2013.

[24] L. Yang, "Depression strategy of IGBT junction temperature fluctuation of power modules FPR wind power converter," M.S. thesis, Dept. Electron. Eng., Chongqing Univ., Chongqing, China, 2016.

[25] M. Akbari, M. T. Bina, A. S. Bahman, B. Eskandari, E. Pouresmaeil, and F. Blaabjerg, "An extended multilayer thermal model for multichip IGBT modules considering thermal aging," *IEEE Access*, vol. 9, pp. 84217–84230, 2021.

[26] L. Xiaohui, R. Weihe, and C. Changsheng, "Newton iterative method for solving nonlinear equation," *Sci. Technol. Wind*, vol. 14, pp. 18–19, May 2021.

[27] A. Jahangiri, M. Mohammadi-Amin, and G. Kahe, "A parametric study on gauss-Newton iterations for wireless sensor network localization," in *Proc. 3rd West Asian Symp. Opt. Millim.-Wave Wireless Commun. (WASOWC)*, Nov. 2020, pp. 1–4.